

# THE OUTFLOWS ACCELERATED BY THE MAGNETIC FIELDS AND RADIATION FORCE OF ACCRETION DISKS

XINWU CAO

Key Laboratory for Research in Galaxies and Cosmology, Shanghai Astronomical Observatory, Chinese Academy of Sciences,  
80 Nandan Road, Shanghai, 200030, China; cxw@shao.ac.cn

accepted by ApJ

## ABSTRACT

The inner region of a luminous accretion disk is radiation pressure dominated. We estimate the surface temperature of a radiation pressure dominated accretion disk,  $\Theta = c_s^2/r^2\Omega_K^2 \ll (H/r)^2$ , which is significantly lower than that of a gas pressure dominated disk,  $\Theta \sim (H/r)^2$ . This means that the outflow can be launched magnetically from the photosphere of the radiation pressure dominated disk only if the effective potential barrier along the magnetic field line is extremely shallow or no potential barrier is present. For the latter case, the slow sonic point in the outflow may probably be in the disk, which leads to a slow circular dense flow above the disk. This implies that hot gas (probably in the corona) is necessary for launching an outflow from the radiation pressure dominated disk, which provides a natural explanation on the observational evidence that the relativistic jets are related to hot plasma in some X-ray binaries and active galactic nuclei. We investigate the outflows accelerated from the hot corona above the disk by the magnetic field and radiation force of the accretion disk. We find that, with the help of the radiation force, the mass loss rate in the outflow is high, which leads to a slow outflow. This may be the reason why the jets in radio-loud narrow-line Seyfert galaxies are in general mild relativistic compared with those in blazars.

*Subject headings:* accretion, accretion disks, galaxies: jets, magnetic fields, galaxies: active

## 1. INTRODUCTION

The acceleration of the gas by the magnetic field lines threading the rotating disks is considered as a promising explanation for jets/outflows observed in different types of the sources, i.e., young stellar objects, X-ray binaries, and active galactic nuclei (AGNs) (see reviews in Spruit 1996; Konigl & Pudritz 2000; Pudritz et al. 2007; Spruit 2010). In this model, a fraction of gas is driven from the disk along the field line co-rotating with the disk by the centrifugal force (Blandford & Payne 1982). The jets/outflows are dominantly powered by the rotational kinetic energy of the disk through the ordered large scale field threading the accretion disk.

It has been also suggested that the outflow can be accelerated by the radiation pressure of the disk (e.g., Bisnovatyi-Kogan & Blinnikov 1977; Shlosman et al. 1985; Murray et al. 1995). This scenario is attractive especially for the jets in the sources accreting at high mass rates. Indeed, jets have been observed in the black hole systems accreting at high rates, such as, some narrow-line Seyfert I galaxies (NLS1s), young radio galaxies, and microquasars (e.g., Zhou et al. 2003; Doi et al. 2006; Yuan et al. 2008; Gu & Chen 2010; Czerny et al. 2009; Wu 2009; Fender et al. 2004). The radiation pressure may also play an important role in the magnetically driven outflows especially from luminous accretion disks. Proga (2000) performed numerical simulations on the radiation-driven outflows from a luminous Keplerian accretion disk threaded by a strong large-scale ordered magnetic field. It has been found that the radiation force is essential in driving outflows from the disk if the thermal energy of the gas is low or the field lines make an angle greater than  $60^\circ$  with respect to the disk midplane. Strictly speaking, the circular motion of the gas in the accretion disk always deviates from Keplerian motion in the presence of a large scale magnetic field, which usually exerts a radial force against the gravitation of the central object. Therefore, the accretion disk threaded by ordered magnetic field lines is therefore always

sub-Keplerian (Ogilvie & Livio 1998, 2001; Cao & Spruit 2002; Cao 2012). The radiation-magnetohydrodynamic simulations have been carried out on the global structure of the accretion disks and outflows around black holes (e.g., Moscibrodzka et al. 2007; Mościbrodzka et al. 2009; Mościbrodzka & Proga 2009; Takeuchi et al. 2010; Ohsuga & Mineshige 2011; Vaidya et al. 2011). It is found that the magnetic force, together with the radiation force exerted by accretion disks, can efficiently drive outflows from luminous accretion disks. Cao (2012) investigated the launching condition for the cold outflows driven by the magnetic field and radiation force of an accretion disk, in which the disk is sub-Keplerian due to the force exerted by the magnetic field. It has been found that the force exerted by the radiation from the disk does help to launch the outflow. The cold gas can be driven from the disk surface even if the field line is inclined at angle greater than  $60^\circ$  with respect to the disk surface, which is obviously different from the pure magnetically driven cold outflow (Blandford & Payne 1982).

In this work, we explore the outflow accelerated from the hot corona above the disk by the magnetic field and radiation force of the disk. In our model, the disk structure, especially the circular motion velocity of the gases in the disk, is altered in the presence of a strong large-scale ordered magnetic field threading the disk. We describe the model and results in Sections 2 and 3, and the discussion is in Sections 4. The final section contains a summary.

## 2. MODEL

We consider the outflow accelerated by the large scale magnetic field and the radiation force of a radiation pressure dominated accretion disk. The rotational velocity of the gas in the disk is sub-Keplerian in the presence of a magnetic field, due to a radial magnetic force against the gravity of the central object. The outflow is fed by the gas at the

disk surface. The properties of the transition region between the disk and outflow are still quite uncertain, though some efforts have been devoted on this issue (e.g., Ogilvie & Livio 1998, 2001). In this work, we consider the outflows fed by the hot corona above the disk, and the temperature and density of the corona are described as the input model parameters. A large scale magnetic field threading the disk is a key ingredient in our model calculations, however, the origin of such a field is still not well understood. The field can be advected inwards by the accretion matter from the interstellar medium or a companion star (Bisnovaty-Kogan & Ruzmaikin 1974, 1976). The inward advection of the field lines is balanced by the outward movement of field lines caused by magnetic diffusion (e.g., van Ballegoijen 1989; Lubow et al. 1994). In principle, the field configuration can be calculated if the structure of the disk is known. Lubow et al. (1994) found that the advection of the field in a conventional viscously driven thin accretion disk is rather inefficient. It was argued that the accretion velocity of the gas in the region away from the mid-plane of the disk can be larger than that at the midplane of the disk, which makes the field dragged in by the accretion disk more efficiently (Lovelace et al. 2009; Guilet & Ogilvie 2012, 2013). Cao & Spruit (2013)'s calculations show that the external field can be advected inwards efficiently if the angular momentum of the disk is predominately removed by the outflows. An alternative for the origin of magnetic fields is the dynamo processes in the disks, and the outflows can be driven by the dynamo generated magnetic fields of the disks (von Rekowski et al. 2003; Campbell 2003). To avoid the complexity of the detailed physics of the disk field formation, we use an analytic magnetic field configuration of an accretion disk given in Cao & Spruit (1994) to investigate the dynamics of the outflow driven by the magnetic field and radiation pressure of the disk.

### 2.1. Structure of a radiation pressure dominated accretion disk

The structure of a radiation pressure dominated accretion disk with a large scale magnetic field has been studied in detail by Cao (2012). We briefly summarize the main results in this subsection.

The half-thickness  $H_d$  of a radiation pressure dominated accretion disk is estimated by assuming the vertical component of gravity to be balanced with the radiation force and the vertical component magnetic force at the disk surface. The curvature of the field line at the disk surface is usually very small, and the vertical magnetic force can be neglected compared with the radiation force at  $z = H_d$ . The disk thickness can be calculated with

$$\frac{GMH_d}{(r_1^2 + H_d^2)^{3/2}} = \frac{f_{\text{rad}}\kappa_{\text{T}}}{c}, \quad (1)$$

where  $f_{\text{rad}}$  is the flux from the unit surface area of the disk, and  $\kappa_{\text{T}}$  is the Thompson scattering cross-section.

The angular velocity  $\Omega$  of the disk is calculated with

$$r_1\Omega_{\text{K}}^2 - r_1\Omega^2 = \frac{B_r^S B_z}{2\pi\Sigma_d r_1} = \frac{B_z^2}{2\pi\Sigma_d r_1 \kappa_0}, \quad (2)$$

where  $B_r^S$  and  $B_z$  are the radial and vertical components of the field at the disk surface, respectively,  $\kappa_0 = B_z/B_r^S$ , and  $\Sigma_d$  is the surface density of the disk. The footpoint of the field line at the disk surface is located at  $r = r_1$  and  $z = H_d$ .

The pressure at the mid-plane of an accretion disk is

$$p_d = \frac{4\sigma}{3c} T_c^4, \quad (3)$$

where  $T_c$  is the central temperature of the disk. The flux radiated from the unit area of the disk surface is related to the temperature and density of the disk by

$$f_{\text{rad}} = \frac{8\sigma T_c^4}{3\Sigma_d \kappa_{\text{T}}}. \quad (4)$$

Substituting Equations (1), (3), and (4) into Equation (2), we find

$$1 - \tilde{\Omega}^2 = \frac{2\beta\tilde{H}_d}{\kappa_0(1 + \tilde{H}_d^2)^{3/2}}, \quad (5)$$

where the dimensionless quantities  $\tilde{\Omega}$ ,  $\tilde{H}_d$ , and  $\beta$ , are defined as

$$\tilde{\Omega} = \frac{\Omega}{\Omega_{\text{K}}}; \quad \Omega_{\text{K}} = \left(\frac{GM}{r_1^3}\right)^{1/2}; \quad \tilde{H}_d = \frac{H}{r_1}; \quad \beta = \frac{B_z^2}{8\pi}/p_d. \quad (6)$$

### 2.2. Magnetic field configuration

We use a magnetic field configuration with

$$B_z(r, z=0) = \left[1 + \left(\frac{r}{r_0}\right)^2\right]^{-1/2}, \quad (7)$$

at the mid-plane of the disk (Cao & Spruit 1994), which is similar to the self-similar disk given in Blandford & Payne (1982) (see Spruit 1996, for the detailed discussion). The stream function of the potential field in the space above/below the disk satisfying the boundary condition (7) is given by

$$\Phi = \left[ \left(\frac{r}{r_0}\right)^2 + \left(1 + \left|\frac{z}{r_0}\right|\right)^2 \right]^{1/2} - \left(1 + \left|\frac{z}{r_0}\right|\right). \quad (8)$$

It satisfies the conditions  $\nabla \times \mathbf{B} = \mathbf{0}$  and  $\nabla \cdot \mathbf{B} = \mathbf{0}$ , and it is used in this work to study the dynamics of the outflow above the disk. The components of the field in the space above the disk are given by

$$B_z(r, z) = \frac{1}{r} \frac{\partial \Phi}{\partial r}, \quad (9)$$

and

$$B_r(r, z) = -\frac{1}{r} \frac{\partial \Phi}{\partial z}. \quad (10)$$

In principle, the radial magnetic field will be sheared into azimuthal field by the differential rotation of the gas in the disk, which leads to magnetorotational instability (MRI) and the MRI-driven turbulence (Balbus & Hawley 1991, 1998). This is the most promising mechanism for angular momentum transportation in accretion disks. In this work, we consider the properties of the disk as the boundary conditions for driving the outflows, and therefore we do not need to consider the detailed physics of the azimuthal field in the disk caused by the differential rotation.

### 2.3. Radiation of the accretion disk

The radiation force exerted by the disk is in  $z$ -direction at the disk surface, which can be determined locally,  $\mathcal{F}_{\text{rad}}(z = H_d) = f_{\text{rad}}\kappa_{\text{T}}\rho_i/c$ , where  $\rho_i$  is the density of the gas at

the disk surface. In the space above the disk, the radiation force exerted by the disk has to be calculated by integrating over the contribution from the whole disk (Bisnovaty-Kogan & Blinnikov 1977).

The  $r$  and  $z$ -components of the radiation force exerted on the gas element with density  $\rho$  at  $(r, z)$  above the disk are

$$\mathcal{F}_{\text{rad},r}(r, z) = \frac{\kappa_{\text{T}}\rho}{c} \times \int_{r'} \int_{\phi'} \frac{f_{\text{rad}}(r')\mu'(1-\mu'^2)^{1/2}(r-r'\cos\phi')}{\pi l(h^2+l^2)} r' dr' d\phi', \quad (11)$$

and

$$\mathcal{F}_{\text{rad},z}(r, z) = \frac{\kappa_{\text{T}}\rho}{c} \int_{r'} \int_{\phi'} \frac{f_{\text{rad}}(r')h^2}{\pi(h^2+l^2)^2} r' dr' d\phi', \quad (12)$$

where

$$h = z - \tilde{H}_{\text{d}}r,$$

$$l = [(r-r'\cos\phi')^2 + r'^2 \sin^2\phi']^{1/2},$$

and

$$\mu' = \frac{h}{(h^2+l^2)^{1/2}}.$$

We have assumed that the relative disk half-thickness  $\tilde{H}_{\text{d}}$  remains constant with radius for a thin disk, which is taken as an input parameter in our model. The flux from the unit surface of a standard thin disk is roughly  $f_{\text{rad}}(r) \propto r^{-3}$  (Shakura & Sunyaev 1973). A pseudo potential  $\Psi_{\text{rad}}$  contributed by the radiation force along the field line is defined as

$$\Psi_{\text{rad}} = -\frac{c}{\kappa_{\text{T}}\rho} \int \mathcal{F}_{\text{rad},r} dr - \frac{c}{\kappa_{\text{T}}\rho} \int \mathcal{F}_{\text{rad},z} dz, \quad (13)$$

which are integrated along the field line from the disk surface. The field line shape is described by Equation (8) with a specified value of  $\Phi$ . Substitute Equation (1) into Equations (11), we can re-write these two equations in dimensionless form,

$$\begin{aligned} \tilde{\mathcal{F}}_{\text{rad},r}(r, z) &= \mathcal{F}_{\text{rad},r}(r, z) \frac{cr_i^2}{GM\kappa_{\text{T}}\rho} \\ &= \frac{1}{\pi} \int_{r'} \int_{\phi'} \frac{\mu'(1-\mu'^2)^{1/2}(r-r'\cos\phi')\tilde{H}_{\text{d}}}{l(h^2+l^2)(1+\tilde{H}_{\text{d}}^2)^{3/2}} \left(\frac{r_i}{r'}\right)^3 r' dr' d\phi', \end{aligned} \quad (14)$$

and

$$\begin{aligned} \tilde{\mathcal{F}}_{\text{rad},z}(r, z) &= \mathcal{F}_{\text{rad},z}(r, z) \frac{cr_i^2}{GM\kappa_{\text{T}}\rho} \\ &= \frac{1}{\pi} \int_{r'} \int_{\phi'} \frac{h^2\tilde{H}_{\text{d}}}{(h^2+l^2)^2(1+\tilde{H}_{\text{d}}^2)^{3/2}} \left(\frac{r_i}{r'}\right)^3 r' dr' d\phi', \end{aligned} \quad (15)$$

where  $r_i$  is the footpoint of the field line at the disk surface. The dimensionless pseudo potential along a magnetic field line contributed by the radiation force is

$$\tilde{\Psi}_{\text{rad}}(\tilde{r}, \tilde{z}) = \Psi_{\text{rad}}(r, z) \frac{r_i}{GM} = -\int \tilde{\mathcal{F}}_{\text{rad},r} d\tilde{r} - \int \tilde{\mathcal{F}}_{\text{rad},z} d\tilde{z}, \quad (16)$$

where  $\tilde{r} = r/r_i$  and  $\tilde{z} = z/r_i$ .

#### 2.4. Outflows driven by the magnetic field and radiation pressure

An isothermal outflow driven by the magnetic field and radiation force of the disk along the field line is described by the following Equations (cf. Cao & Spruit 1994):

$$p = \rho c_{\text{s},i}^2, \quad (17)$$

$$v_{\text{p}} = \frac{f}{\rho} B_{\text{p}}, \quad (18)$$

$$(v_{\phi} - \Omega r) B_{\text{p}} = v_{\text{p}} B_{\phi}, \quad (19)$$

$$r \left( v_{\phi} - \frac{B_{\text{p}} B_{\phi}}{4\pi\rho v_{\text{p}}} \right) = \Omega r_{\text{A}}, \quad (20)$$

and

$$\frac{v_{\text{p}}^2}{2} + \frac{1}{2}(v_{\phi} - \Omega r)^2 + c_{\text{s},i}^2 \ln \frac{\rho}{\rho_{\text{A}}} + \Psi_{\text{eff}}(r, z) = E, \quad (21)$$

where the effective potential along the field line threading the accretion disk with angular velocity  $\Omega$  at the field footpoint  $r_i$  is

$$\Psi_{\text{eff}}(r, z) = -\frac{GM}{(r^2+z^2)^{1/2}} - \frac{1}{2}\Omega(r_i)^2 r^2 + \Psi_{\text{rad}}(r, z). \quad (22)$$

The last term in Equation (22) is contributed by the radiation force from the disk (see Equation 13). Equation (18) is the mass conservation of the outflow along the field line, where  $v_{\text{p}}$  and  $B_{\text{p}}$  are the poloidal velocity and field strength respectively, and  $f$  describes the mass loss rate in the outflow. The conservation of angular momentum is described by Equation (20), in which  $r_{\text{A}}$  is the Alfvén radius of the outflow. The field line and the motion of the outflow are parallel in the co-rotating field line frame (Equation 19). Equation (21) is the Bernoulli Equation of the isothermal outflow.

Substituting Equations (17)-(20) into Equation (21), we have

$$\begin{aligned} H(r, \rho, r_{\text{A}}, \rho_{\text{A}}) &= \frac{B_{\text{p}}^2}{8\pi\rho_{\text{A}}} \left( \frac{\rho_{\text{A}}}{\rho} \right)^2 + \frac{\Omega^2(r_{\text{A}}^2 - r^2)^2}{2r^2(1-\rho/\rho_{\text{A}})^2} \\ &+ c_{\text{s},i}^2 \ln \frac{\rho}{\rho_{\text{A}}} + \Psi_{\text{eff}} = E, \end{aligned} \quad (23)$$

where  $c_{\text{s},i}$  is the sound speed of the gas at the disk surface/the bottom of the outflow, and  $\rho_{\text{A}}$  is the density of the outflow at the Alfvén radius  $r_{\text{A}}$ . It can be re-written in dimensionless form as

$$\begin{aligned} \tilde{H}(x, y, x_i, y_i) &= \frac{r_i}{GM} H(r, \rho, r_{\text{A}}, \rho_{\text{A}}) \\ &= \frac{\beta_i y_i \Theta_i}{y^2} + \frac{(1-x^2)^2 \tilde{\Omega}^2}{2x^2 x_i^2 (1-y)^2} + \Theta_i \ln y + \tilde{\Psi}_{\text{eff}} = \tilde{E}, \end{aligned} \quad (24)$$

where

$$x = r/r_{\text{A}}; \quad y = \rho/\rho_{\text{A}}; \quad \Theta_i = \frac{c_{\text{s},i}^2}{r_i^2 \Omega_{\text{K}}^2};$$

$$\beta_i = \frac{B_{\text{p},i}^2}{8\pi} / p_i = \frac{B_{\text{p},i}^2}{8\pi} / \rho_i c_{\text{s},i}^2, \quad (25)$$

and the subscripts ‘‘i’’ refer to the values of the quantities at the bottom of the outflow.

Substituting Equation (1) into Equation (22), the effective potential along the field line threading the accretion disk with

angular velocity  $\Omega$  at radius  $r_i$  can be re-written in dimensionless form,

$$\tilde{\Psi}_{\text{eff}}(\tilde{r}, \tilde{z}) = \Psi_{\text{eff}}(r, z) \frac{r_i}{GM} = -\frac{1}{(\tilde{r}^2 + \tilde{z}^2)^{1/2}} - \frac{1}{2} \tilde{\Omega}^2 \tilde{r}^2 + \tilde{\Psi}_{\text{rad}}(\tilde{r}, \tilde{z}), \quad (26)$$

where  $\tilde{r} = r/r_i$ ,  $\tilde{z} = z/r_i$ , and the last term is calculated with Equation (16).

For a given magnetic field configuration, the outflow along a field line passes through three critical points, i.e., the slow sonic, Alfvén, and fast sonic points (Sakurai 1985; Cao & Spruit 1994). At the two sonic points, the function  $\tilde{H}(x, y, x_i, y_i)$  satisfies

$$\frac{\partial \tilde{H}}{\partial x} = \frac{\partial \tilde{H}}{\partial y} = 0, \quad (27)$$

and

$$\tilde{H}(x_s, y_s, x_i, y_i) = \tilde{H}(x_f, y_f, x_i, y_i) = \tilde{E}. \quad (28)$$

An additional condition,

$$\tilde{H}(x, y, x_i, y_i) = \tilde{E}, \quad (29)$$

is imposed at the disk surface, i.e.,  $x = x_i$ ,  $y = y_i$ . A set of seven Equations (27), (28), and (29), can be solved for seven variables,  $x_s, y_s, x_f, y_f, x_i, y_i$ , and  $\tilde{E}$ , for an outflow along a given magnetic field line, when the temperature and density of the gas at the bottom of the outflow are specified.

With the derived outflow solution, the mass loss rate in the outflow from the unit surface area is available,

$$\dot{m}_w = \rho_i v_{p,i} \frac{B_z}{B_{p,i}} = \rho_i v_{p,i} \frac{\kappa_0}{(1 + \kappa_0^2)^{1/2}}, \quad (30)$$

which can be re-written in dimensionless form as

$$\frac{\dot{m}_w}{\Sigma_d \Omega_K} = \frac{\beta \tilde{H}_d (1 + \kappa_0^2)^{1/2}}{\kappa_0 [2\beta_i \Theta_i y_i (1 + \tilde{H}_d^2)^3]^{1/2}}. \quad (31)$$

Here, Equations (1), (3), (4) and (24) are used. The reciprocal of  $\dot{m}_w / \Sigma_d \Omega_K$  represents the number of orbits in which all the gas in the disk is channeled into the outflow.

### 2.5. Boundary conditions

The solution of an outflow along a given field line is available by solving a set of seven non-linear algebraic equations with suitable boundary conditions at the disk surface. The dimensionless temperature  $\Theta_i$  of the gas is an input parameter, and the density of the gas is described by  $\beta_i$  if the value of  $\beta$  is specified (see Equation 25). For the outflow can be efficiently driven by the magnetic field, the gas pressure should be lower than the magnetic pressure, i.e.,  $\beta_i \gtrsim 1$  is required. For most calculations in this work,  $\beta_i = 1$  is used.

The temperature of the photosphere roughly equals to the surface temperature of the disk,  $T_i$ , which is given by

$$T_i = \frac{f_{\text{rad}}^{1/4}}{\sigma^{1/4}}. \quad (32)$$

The sound speed of the gas in the photosphere of the disk is

$$c_{s,i} = \left( \frac{kT_i}{\mu m_p} \right)^{1/2}. \quad (33)$$

Substituting Equations (1) and (32) into Equation (33), we have

$$\begin{aligned} \frac{c_{s,i}^2}{r_i^2 \Omega_K^2} &= \left[ (1.895 M_\odot)^2 \frac{60 G^3}{\pi^2 \kappa_T} \frac{r_i \Omega_K^2 \tilde{H}_d}{(1 + \tilde{H}_d^2)^{3/2}} \right]^{1/4} \frac{r_i}{GM \mu} \\ &= 4.946 \times 10^{-6} \mu^{-1} (r_i/r_s)^{1/2} \tilde{H}_d^{1/4} m^{-1/4} (1 + \tilde{H}_d^2)^{-3/8}, \end{aligned} \quad (34)$$

where

$$r_s = \frac{2GM}{c^2}, \quad m = \frac{M}{M_\odot}, \quad (35)$$

and  $(\hbar c/G)^{3/2} m_p^{-2} = 1.895 M_\odot$  is used. The molecular weight  $\mu = 0.5$  for pure hydrogen plasma.

The surface temperature of a gas pressure dominated accretion disk is

$$\frac{c_{s,i}^2}{r_i^2 \Omega_K^2} = \left( \frac{4}{3\tau} \right)^{1/4} \frac{c_{s,c}^2}{r_i^2 \Omega_K^2} = \left( \frac{4}{3\tau} \right)^{1/4} \tilde{H}_d^2, \quad (36)$$

where  $c_{s,c}$  is the sound speed of the gas at the mid-plane of the disk, and  $\tau$  is the optical depth of the disk in the vertical direction. The optical depth  $\tau$  is in the range of  $\sim 10^2 - 10^5$  for a thin accretion disk accreting at different rates, which means the surface temperature of the disk,  $c_{s,i}^2 / r_i^2 \Omega_K^2 \sim 0.06 - 0.34 \tilde{H}_d^2$  (Cao & Spruit 2013). Compared with a gas pressure dominated accretion disk, the surface temperature of a radiation pressure dominated accretion disk is much lower,  $c_{s,i}^2 / r_i^2 \Omega_K^2 \ll \tilde{H}_d^2$  (see Equation 34). The accretion disk is gas pressure dominated in the outer region or/and its mass accretion rate is low (Laor & Netzer 1989; Shakura & Sunyaev 1973). This implies gas pressure gradient in the outflow from the inner region of a luminous (radiation pressure dominated) disk is almost negligible, and therefore the cold gas approximation is a good approximation (Cao 2012). In this case, the outflow will be suppressed if the field line is inclined at an angle slightly larger than the critical one, because the internal energy of such cold gas at the disk surface is too low to overcome the effective potential barrier along the field line. If the angle is lower than the critical one, the slow sonic point may probably go into the disk, and the density of the gas in the disk is usually high, which usually leads to a slow dense circular flow above the disk (see Cao & Spruit 1994; Spruit 1996, for the detailed discussion). It implies that hot gas is needed for feeding an outflow from a radiation pressure dominated accretion disk.

The observed ultraviolet (UV)/optical emission of AGN is thought to be the thermal emission from the standard geometrically thin, optically thick accretion disks (e.g., Shields 1978; Malkan & Sargent 1982; Sun & Malkan 1989). The observed power-law hard X-ray spectra of AGN are most likely due to the inverse Compton scattering of soft photons on a population of hot electrons in the coronas above the disk (Galeev et al. 1979; Haardt & Maraschi 1993; Haardt et al. 1994). It has been found that the temperature of the hot electrons in the corona is roughly around  $10^9$  K, which can successfully reproduce a power-law hard X-ray spectrum as observed (e.g., Liu et al. 2003; Cao 2009). In this work, we consider a hot corona above a thin accretion disk, which is a reservoir to supply hot gas to feed the outflow driven by the magnetic field and radiation force of the disk. The detailed properties of the corona are still quite unclear. For simplicity, we use two parameters, the temperature  $\Theta_i$  and the density of the corona, in our model calculations. As the magnetic

field strength at the disk surface is described by the value of  $\beta$  specified, the density of the corona is given by the ratio of magnetic to gas pressure in the corona ( $\beta_i$ ) for given temperature  $\Theta_i$  and disk field strength  $\beta$  (see Equation 25).

### 3. RESULTS

We compare the temperatures of the photospheres between the radiation pressure dominated disks and gas pressure dominated accretion disks in Figure 1. As discussed in Section 2.5, the temperature of the photosphere of a radiation pressure dominated accretion disk is indeed much lower than that of a gas pressure dominated accretion disk. We note that the surface temperature of the radiation pressure dominated disk decreases with increasing black hole mass.

We use the magnetic field configuration above the disk given in Section 2.2, of which the field line is given by setting  $\Phi = \text{const}$ . In our calculations, the relative disk thickness  $\tilde{H}_d$  is assumed to be independent of radius, which is an input parameter. The angular velocity of the disk can be calculated with Equation (5), if the strength of the magnetic field  $\beta$  at the disk surface, the disk thickness  $\tilde{H}_d$ , and the field line inclination  $\kappa_0$  are specified. The field line inclination  $\kappa_0$  at the disk surface is a function of  $r/r_0$ .

With the specified values of  $\Theta_i$  and  $\beta_i$  of the corona, we can calculate the dynamics of the outflow along a given magnetic field line as described in Section 2. In Figures 2-4, we plot the location of the critical points in the outflow solutions derived with different values of the model parameters. We show how the results vary with the magnetic field strength  $\beta$  in Figure 2. The rotational velocity  $\Omega$  of the disk decreases with increasing field strength  $\beta$  (see Equation 5), and the effective potential barrier increases with decreasing  $\tilde{\Omega}$ . Thus, the critical points go far away from the disk. In Figure 3, we plot the results calculated with different values of corona temperature  $\Theta_i$ . In order to show the role of the radiation force on the acceleration of the outflows, we compare the results with those of the purely magnetically driven outflows in Figure 4. The location of the critical points in the pure magnetically driven outflows is farther away from the disk compared with those of the outflows driven by the magnetic field together with the radiation force. This is because the effective potential barrier becomes deep for a pure magnetically driven outflow (see Figure 5).

We can calculate the mass loss rate in the outflow with Equation (31) when the outflow solution is derived. In Figures 6, we plot the mass loss rates as functions of the field line inclination  $\kappa_0$  at the disk surface. The velocities of the outflows along the field lines are given in Figures 7 and 8. The mass loss rates decrease with  $\kappa_0$ , while the velocities of the outflows increase with the field line inclination  $\kappa_0$  (see Figures 6-8). We find that the dynamical properties of the outflows are different near the disk surface, while the poloidal velocities converge at large distances along the field lines with the same  $\kappa_0$  for low- $\kappa_0$  case. It is found that the velocities of the flows increase with decreasing density of the corona (large- $\beta_i$ ), if the values of all the other parameters are fixed (see Figures 7 and 8).

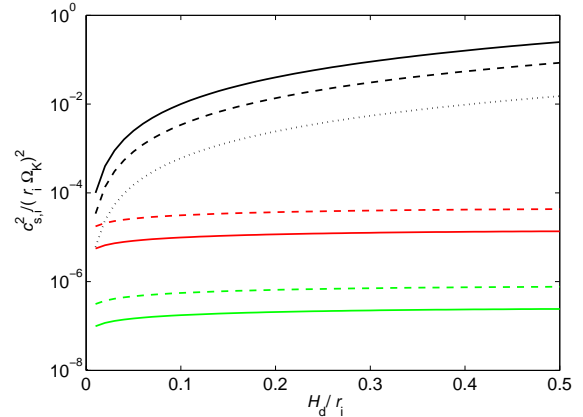


FIG. 1.— The temperature of the photosphere of the disk. The coloured lines represent the results for radiation pressure dominated accretion disks (see Section 2.5 for the detailed discussion). The red lines are the results calculated with a black hole mass  $M = 10M_\odot$ , while the green lines are for a massive black hole with  $M = 10^8M_\odot$ . The solid lines indicate the temperature at radius  $r = 10r_s$ , and the dashed lines are for  $r = 100r_s$ . The black solid line represent the temperature of the photosphere of an isothermal gas pressure dominated accretion disk, while the dashed and dotted lines are the results calculated with  $\tau = 100$  and  $10^5$ , respectively.

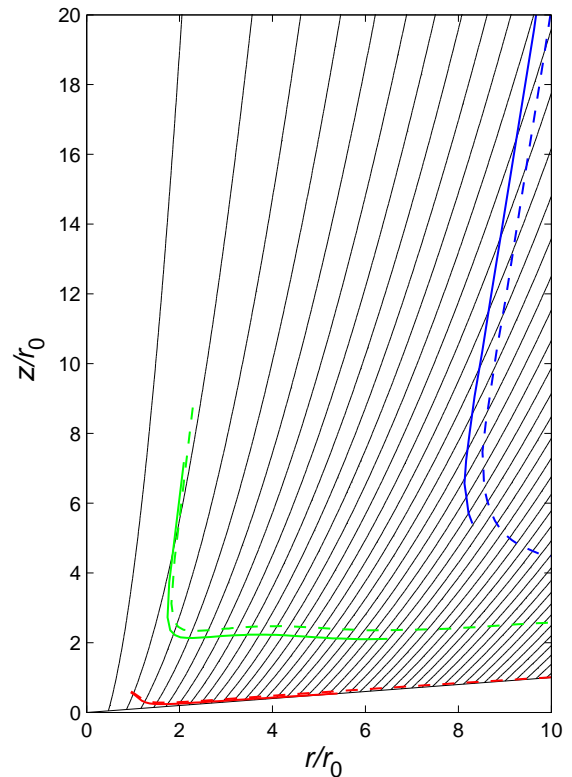


FIG. 2.— The locations of the critical points of the outflow solutions (red: slow sonic points; green: Alfvén points; blue: fast sonic points). The disk thickness  $\tilde{H}_d = 0.1$ , the dimensionless temperature of the hot corona  $\Theta_i = 0.01$ , and the ratio of magnetic to gas pressure in the corona  $\beta_i = 1$ , are adopted in the calculations. Different types of lines represent the results for different values of  $\beta = 0.75$  (solid) and 1 (dashed), respectively.

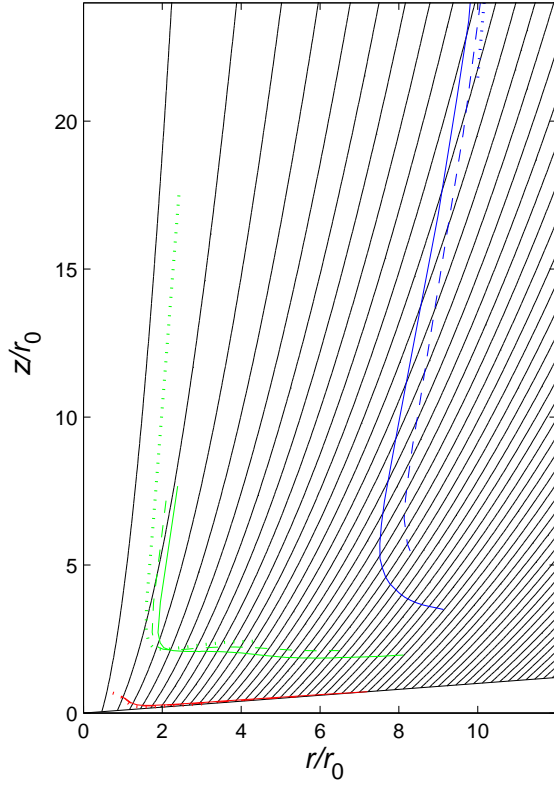


FIG. 3.— The same as Figure 2. In all calculations,  $\beta = 0.75$  is adopted. Different types of lines represent the results for different values of  $\Theta_i = 0.005$  (solid),  $0.01$  (dashed), and  $0.02$  (dotted), respectively.

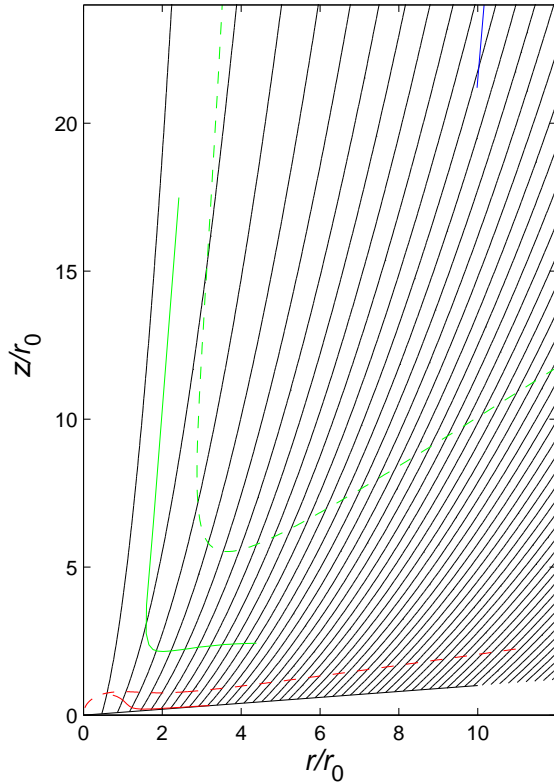


FIG. 4.— The locations of the critical points of the outflow solutions (red: slow sonic points; green: Alfvén points; blue: fast sonic points). The disk thickness  $\tilde{H}_d = 0.1$ , the dimensionless temperature of the hot corona  $\Theta_i = 0.02$ , and the ratio of magnetic to gas pressure in the corona  $\beta_i = 1$ , and  $\beta = 0.75$  are adopted in the calculations. For comparison, the results without considering the effects of radiation pressure are also plotted (dashed lines).

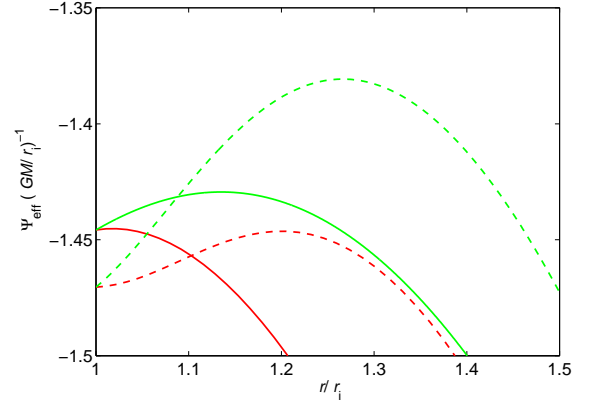


FIG. 5.— The effective potential along the field line threading a disk with  $\tilde{H}_d = 0.1$  and  $\beta = 0.75$ . The solid lines represent the results for the field line inclination  $\kappa_0 = 1.5$  at the disk surface, while the dashed lines are for  $\kappa_0 = 3$ . For comparison, we plot the results calculated without considering radiation pressure effects as green lines.

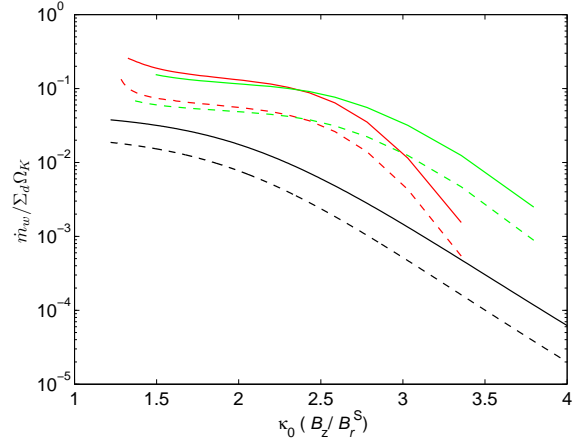


FIG. 6.— The dimensionless mass loss rates in the outflows as functions of field line inclination  $\kappa_0 = B_z/B_r^S$  at the disk surface. In all the calculations,  $\beta = 0.75$  and  $\tilde{H}_d = 0.1$  are adopted. The solid lines represent the results calculated with  $\beta_i = 1.0$ , while the dashed lines are for  $\beta_i = 3$ . The different colors are for different corona temperature,  $\Theta_i = 0.01$  (red) and  $0.02$  (green). For comparison, we plot the result for purely magnetically driven outflows with  $\Theta_i = 0.02$  as black lines (solid line:  $\beta_i = 1$ , and dashed lines:  $\beta_i = 3$ ).

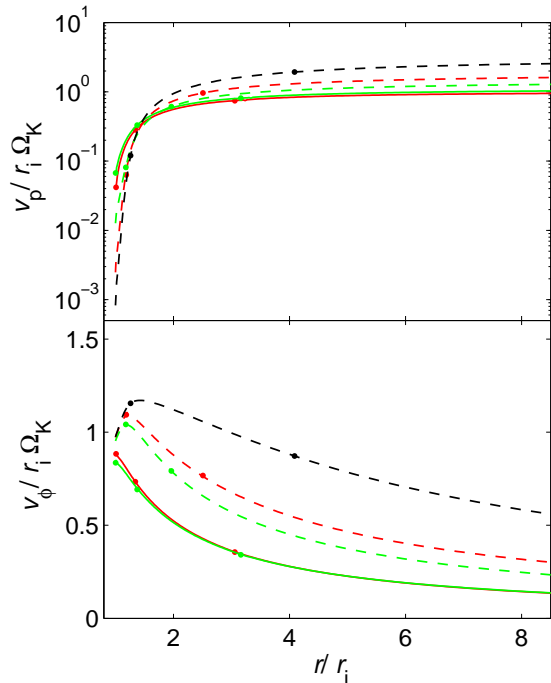


FIG. 7.— The poloidal and azimuthal velocities of the outflow along the field line. The ratio of magnetic to gas pressure in the corona  $\beta_i = 1$ , and  $\beta = 0.75$ , are adopted in all the calculations. The solid lines represent the outflow along the field line with  $\kappa_0 = 1.5$  at the disk surface, while the dashed lines are for  $\kappa_0 = 3$ . The colored lines represent for the results with different values of model parameters (red lines:  $\Theta_i = 0.01$ , and green lines:  $\Theta_i = 0.02$ ). The black dashed lines are the results calculated with pure magnetically driven outflow model ( $\kappa_0 = 3$  and  $\Theta_i = 0.02$ ). The dots indicate the critical points in the outflow, i.e., slow sonic, Alfvén, and fast sonic points (from left to right).

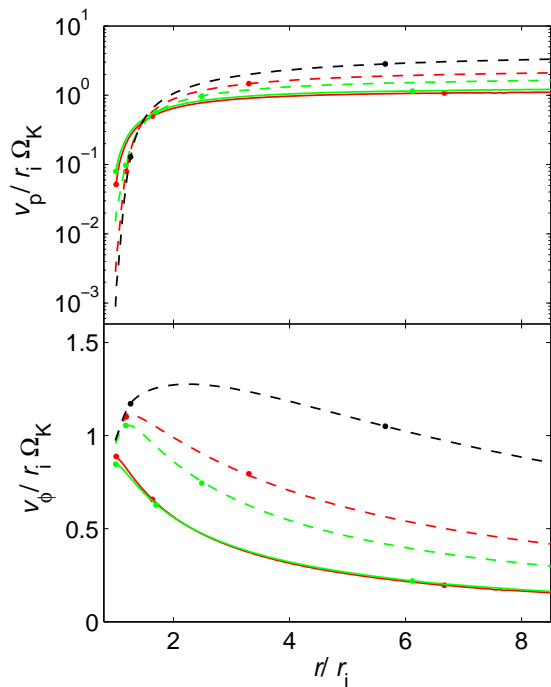


FIG. 8.— The same as Figure 7, but  $\beta_i = 3$  is adopted.

#### 4. DISCUSSION

We find that the temperature of the photosphere at the surface of a radiation pressure disk is significantly lower than

that for a gas pressure dominated accretion disk with the same relative disk thickness  $\tilde{H}_d$  (see Figure 1). The surface temperature of the radiation pressure disk is insensitive to the disk thickness  $H_d/r$ , while it decreases with increasing black hole mass. The gas pressure gradient may help accelerating the outflow. The importance of the gas pressure on driving the outflow can be estimated by comparing  $c_s^2$  with the effective potential barrier  $\Delta\Psi_{\text{eff}} = \Psi_{\text{eff}}^{\text{max}} - \Psi_{\text{eff},i}$  along the field line. In the magnetically driven outflow model, the mass loss rate in the outflow  $\dot{m}_w \propto \exp(-\Delta\Psi_{\text{eff}}/c_s^2)$  (see Spruit 1996; Ogilvie & Livio 1998, for the details). For such a low-temperature photosphere at the surface of the radiation pressure dominated disk, an extremely shallow potential barrier (small- $\Delta\Psi_{\text{eff}}$ ) is required for launching an outflow, which means the values of  $\beta$  and  $\kappa_0$  should be in the narrow ranges close to those of the cold gas launching condition given in Cao (2012). It implies strict constraints on the outflows that can be driven from the disk surface, especially for massive black hole cases, as the temperatures of the spheres are above two orders of magnitude lower than those of stellar black hole accretion disks (see Figure 1). The outflow can be launched along the field line if the effective potential  $\Psi_{\text{eff}}$  monotonically decreases along the field line. In this case, the outflow is alternatively accelerated within the disk, which is, for example, similar to the solutions of the outflows along the field lines inclined at small angles with respect to the disk surface given in Cao & Spruit (1994). The gas overcomes a potential barrier along the field line in the disk, and the slow sonic point is located within the disk. Thus, the slow dense circular flows are usually present above the disks in this case (Cao & Spruit 1994). Such calculations can be done with a known field configuration within the disk, which is beyond the scope of this work, and we will not investigate this kind of solutions in this paper.

As discussed in Section 2.5, the outflow can be driven from the hot gas in the corona above the disk. The field configuration can be derived with the detailed physics of advection and diffusion of magnetic fields considered (van Ballegoijen 1989; Lubow et al. 1994; Lovelace et al. 2009; Guilet & Ogilvie 2012, 2013; Cao & Spruit 2013), which is beyond the scope of this work. We use the configuration of the field given in Section 2.2, of which the strength at the disk surface decreases with increasing radius. As we focus on how the hot gas at the disk surface is accelerated along the field line with the help with the radiation force of the disk, the above mentioned field configuration is sufficient for our present investigation.

The location of the critical points of the outflow solutions with different values of the accretion disk/corona parameters is plotted in Figures 2-4. It is found that the slow sonic points are always close to the disk surface. In the central region of the disk, the field lines are inclined at large angles with respect to the disk surface. The mass loss rate in the outflow decreases with increasing inclination  $\kappa_0$  (see Figure 6), because of the effective potential barrier increases with  $\kappa_0$  (see Figure 5) and  $\dot{m}_w \propto \exp(-\Delta\Psi_{\text{eff}}/c_s^2)$ . The Alfvén and fast sonic points go farther away from the disk when  $\kappa_0$  is large (see Figures 2-4), which is caused by a tenuous low- $\dot{m}_w$  outflow. The mass loss rate in the outflow increases with the temperature  $\Theta_i$  of the gas in the corona, if the values of all other parameters are fixed. In order to illustrate the role of the radiation force on the acceleration of the outflow, we compare the results of pure magnetically driven outflows in Figure 6. The mass loss



rates in the outflows driven by the magnetic field and radiation pressure are significantly higher than those for pure magnetically driven outflows, because the radiation pressure makes the effective potential barrier shallow.

Less mass is loaded in the outflow in high- $\kappa_0$  cases, and the outflow can be driven to a relative high velocity, while a slow dense outflow is present when  $\kappa_0$  is small. It is found that the poloidal velocities of the outflows almost converge at large distances along the field line with a given  $\kappa_0$  for low- $\kappa_0$  cases. This implies that the gas in the dense outflows is dominantly accelerated by the radiation pressure of the disk, which is almost independent of the values of the disk parameters. However, the situation is different for the azimuthal velocity of the outflows, which is independent of the radiation pressure. We find that the outflows with low mass loss rates, i.e., low- $\Theta_1$ , or/and high- $\kappa_0$  as discussed above, can be accelerated to a large velocity in the azimuthal direction.

### 5. SUMMARY

We estimate the temperature of the photosphere above the radiation dominated accretion disk, and find that  $\Theta \ll \tilde{H}_d^2$ . Therefore, it is difficult for the outflows driven from the photospheres of the radiation dominated disks. This implies that hot gas (probably in the corona) is necessary for launching

an outflow from the radiation pressure dominated disk, which provides a natural explanation on the observational evidence that the relativistic jets are related to hot plasma in some X-ray binaries and active galactic nuclei (Zdziarski et al. 2011; Wu et al. 2013).

We investigate the outflows accelerated from the hot corona above the disk by the magnetic field and radiation force of the accretion disk, and find that the outflow can be driven from the corona with the help of radiation force even if the field line is inclined at a large angle ( $> 60^\circ$ ) with respect to the disk surface. The potential barrier decreases due to the radiation force of the disk, and therefore the mass loss rate in the outflow increases. We find that slow outflows with high mass loss rates are present if the field line inclination  $\kappa_0 \lesssim 2$ . This may be the reason why the jets in radio-loud narrow-line Seyfert galaxies are in general mild relativistic compared with those in blazars (Komossa et al. 2006; Doi et al. 2006; Gu & Chen 2010; Doi et al. 2011).

This work is supported by the NSFC (grants 11173043, 11121062, and 11233006), the CAS/SAFEA International Partnership Program for Creative Research Teams (KJCX2-YW-T23), and Shanghai Municipality.

### REFERENCES

- Balbus, S. A., & Hawley, J. F. 1991, *ApJ*, 376, 214  
 Balbus, S. A., & Hawley, J. F. 1998, *Reviews of Modern Physics*, 70, 1  
 Bisnovaty-Kogan, G. S., & Blinnikov, S. I. 1977, *A&A*, 59, 111  
 Bisnovaty-Kogan, G. S., & Ruzmaikin, A. A. 1974, *Ap&SS*, 28, 45  
 Bisnovaty-Kogan, G. S., & Ruzmaikin, A. A. 1976, *Ap&SS*, 42, 401  
 Blandford, R. D., & Payne, D. G. 1982, *MNRAS*, 199, 883  
 Campbell, C. G. 2003, *MNRAS*, 345, 123  
 Cao, X. 2009, *MNRAS*, 394, 207  
 Cao, X. 2012, *MNRAS*, 426, 2813  
 Cao, X., & Spruit, H. C. 1994, *A&A*, 287, 80  
 Cao, X., & Spruit, H. C. 2002, *A&A*, 385, 289  
 Cao, X., & Spruit, H. C. 2013, *ApJ*, 765, 149  
 Czerny, B., Siemiginowska, A., Janiuk, A., Nikiel-Wroczyński, B., & Stawarz, Ł. 2009, *ApJ*, 698, 840  
 Doi, A., Asada, K., & Nagai, H. 2011, *ApJ*, 738, 126  
 Doi, A., Fujisawa, K., Habe, A., et al. 2006, *PASJ*, 58, 777  
 Fender, R. P., Belloni, T. M., & Gallo, E. 2004, *MNRAS*, 355, 1105  
 Galeev, A. A., Rosner, R., & Vaiana, G. S. 1979, *ApJ*, 229, 318  
 Gu, M., & Chen, Y. 2010, *AJ*, 139, 2612  
 Guilet, J., & Ogilvie, G. I. 2012, *MNRAS*, 424, 2097  
 Guilet, J., & Ogilvie, G. I. 2013, *MNRAS*, 430, 822  
 Haardt, F., & Maraschi, L. 1993, *ApJ*, 413, 507  
 Haardt, F., Maraschi, L., & Ghisellini, G. 1994, *ApJ*, 432, L95  
 Koide, S., Shibata, K., & Kudoh, T. 1999, *ApJ*, 522, 727  
 Komossa, S., Voges, W., Xu, D., et al. 2006, *AJ*, 132, 531  
 Konigl, A., & Pudritz, R. E. 2000, *Protostars and Planets IV*, 759  
 Laor, A., & Netzer, H. 1989, *MNRAS*, 238, 897  
 Liu, B. F., Mineshige, S., & Ohsuga, K. 2003, *ApJ*, 587, 571  
 Lovelace, R. V. E., Rothstein, D. M., & Bisnovaty-Kogan, G. S. 2009, *ApJ*, 701, 885  
 Lubow, S. H., Papaloizou, J. C. B., & Pringle, J. E. 1994, *MNRAS*, 267, 235  
 Malkan, M. A., & Sargent, W. L. W. 1982, *ApJ*, 254, 22  
 Mościbrodzka, M., Gammie, C. F., Dolence, J. C., Shiokawa, H., & Leung, P. K. 2009, *ApJ*, 706, 497  
 Mościbrodzka, M., & Proga, D. 2009, *MNRAS*, 397, 2087  
 Moscibrodzka, M., Proga, D., Czerny, B., & Siemiginowska, A. 2007, *A&A*, 474, 1  
 Murray, N., Chiang, J., Grossman, S. A., & Voit, G. M. 1995, *ApJ*, 451, 498  
 Ogilvie, G. I., & Livio, M. 1998, *ApJ*, 499, 329  
 Ogilvie, G. I., & Livio, M. 2001, *ApJ*, 553, 158  
 Ohsuga, K., & Mineshige, S. 2011, *ApJ*, 736, 2  
 Proga, D. 2000, *ApJ*, 538, 684  
 Proga, D. 2003, *ApJ*, 585, 406  
 Proga, D., & Begelman, M. C. 2003, *ApJ*, 592, 767  
 Proga, D., Stone, J. M., & Kallman, T. R. 2000, *ApJ*, 543, 686  
 Pudritz, R. E., Ouyed, R., Fendt, C., & Brandenburg, A. 2007, *Protostars and Planets V*, 277  
 Sakurai, T. 1985, *A&A*, 152, 121  
 Shakura, N. I., & Sunyaev, R. A. 1973, *A&A*, 24, 337  
 Shields, G. A. 1978, *Nature*, 272, 706  
 Shlosman, I., Vitello, P. A., & Shaviv, G. 1985, *ApJ*, 294, 96  
 Spruit, H. C. 1996, *NATO ASIC Proc. 477, Evolutionary Processes in Binary Stars*, ed. R. A. M. J. Wijers, M. B. Davies, & C. A. Tout (Dordrecht: Kluwer), 249  
 Spruit, H. C. 2010, *The Jet Paradigm*, ed. T. Belloni (Lecture Notes in Physics, Vol. 794; Berlin: Springer), 233  
 Sun, W.-H., & Malkan, M. A. 1989, *ApJ*, 346, 68  
 Takeuchi, S., Ohsuga, K., & Mineshige, S. 2010, *PASJ*, 62, L43  
 Vaidya, B., Fendt, C., Beuther, H., & Porth, O. 2011, *ApJ*, 742, 56  
 van Ballegoijen, A. A. 1989, *Accretion Disks and Magnetic Fields in Astrophysics*, Vol. 156, ed. G. Belvedere (Dordrecht: Kluwer), 99  
 von Rekowski, B., Brandenburg, A., Dobler, W., Dobler, W., & Shukurov, A. 2003, *A&A*, 398, 825  
 Wu, Q. 2009, *ApJ*, 701, L95  
 Wu, Q., Cao, X., Ho, L. C., & Wang, D.-X. 2013, *ApJ*, 770, 31  
 Yuan, W., Zhou, H. Y., Komossa, S., et al. 2008, *ApJ*, 685, 801  
 Zdziarski, A. A., Skinner, G. K., Pooley, G. G., & Lubiński, P. 2011, *MNRAS*, 416, 1324  
 Zhou, H.-Y., Wang, T.-G., Dong, X.-B., Zhou, Y.-Y., & Li, C. 2003, *ApJ*, 584, 147